ЖЭТФ, 2008, том 133, вып. 5, стр. 1017–1026

EXPERIMENTAL STUDY OF MAGNETIC PHASE TRANSITION IN THE ITINERANT HELIMAGNET MnSi

S. M. Stishov[a]*, A. E. Petrova[a], S. Khasanov[b], G. Kh. Panova[c], A. A. Shikov[c], J. C. Lashley[d], D. Wu[e], T. A. Lograsso[e]

[a] *Institute for High Pressure Physics*
142190, Troitsk, Moscow Region, Russia

[b] *Institute of Solid State Physics*
142432, Chernogolovka, Moscow Region, Russia

[c] *Russian Research Center Kurchatov Institute*
123182, Moscow, Russia

[d] *Los Alamos National Laboratory, Los Alamos, 87545 NM, USA*

[e] *Ames Laboratory, Iowa State University, Ames, IA 50011, USA*

Received September 16, 2007

Magnetic susceptibility, heat capacity, thermal expansion and resistivity of a high-quality single crystal of MnSi were carefully studied at ambient pressure. The calculated magnetic entropy change in the temperature range 0–30 K is less than $0.1R$, the low value that emphasizes the itinerant nature of magnetism in MnSi. A linear temperature term dominates behavior of the thermal expansion coefficient in the range 30–150 K, which correlates with great enhancement of the linear electronic term in the heat capacity. Surprising similarity between variation of the heat capacity, the thermal expansion coefficient, and the temperature derivative of resistivity through the phase transition in MnSi is observed. Specific forms of the heat capacity, thermal expansion coefficient, and temperature derivative of resistivity at the phase transition to a helical magnetic state near 29 K are interpreted as a combination of sharp first-order features and broad peaks or shallow valleys of yet unknown origin. The appearance of these broad satellites probably hints at the frustrated magnetic state in MnSi slightly above the transition temperature. Present experimental findings question current views on the phase diagram of MnSi.

PACS: 75.30.Kz, 75.40.Cx, 77.80.Bh

1. INTRODUCTION

Extensive studies of the physical properties of the itinerant helimagnet MnSi that have been carried out for decades brought up a number of intriguing results of general physical significance. Magnetic ordering of unknown nature in MnSi, occurring around 30 K, was reported for the first time in Ref. [1]. The magnetic moment per Mn atom at low temperature was found to equal $0.4\mu_B$, whereas fitting susceptibility data to the Curie–Weiss law gave the effective moment $2.2\mu_B$ per Mn in the paramagnetic phase [2]. This difference is usually considered a signature of the itinerant nature of magnetism.

The crystal structure of MnSi as well as some other silicides and germanides (FeSi, CoSi, FeGe, etc) of the transition metals belongs to the B 20 type, cubic space group (T^4) [3]. The space group $P2_13$ does not contain a center of symmetry that allows a nonzero value of the Dzyaloshinski–Moriya term in energy $D[S_i \times S_j]$, arising from small relativistic spin–lattice and spin–spin interactions [4, 5]. Although this term is small, it could cause a long-wave modulation of the magnetic spin structure. Consistently with theory, a magnetic order in MnSi was identified as a long-period ferromag-

*E-mail: sergei@hppi.troitsk.ru

netic spiral or helical spin structure [6]. At zero magnetic field, the axis or the wave vector q of the helix is directed along a space diagonal of the cubic unit cell of MnSi, and therefore spins are ferromagnetically aligned in layers parallel to the (111) plane. The magnetic moment of each successful layer is turned by a small angle with respect to a previous one, thus forming a spiral with a pitch of 180 Å ($q = 0.035$ Å^{-1}). The wave vector can be aligned in different directions on application of the magnetic field about 0.2 T. At the magnetic field about 0.6 T, a field-induced ferromagnetic structure appears [2]. Therefore, magnetic properties of MnSi are governed by a hierarchy of three energy scales: the exchange interaction, defining in-plane ferromagnetic ordering; the weak Dzyaloshinski–Moriya spin–orbit interaction, producing chirality of the spin structure; and weaker anisotropic exchange crystal anisotropy terms, directing the wave vector q along the space diagonal of the cubic cell.

The order parameter in MnSi has two components, characterizing the spin and chiral orders, and can be described by a complex vector $S = S_0 e^{iqz}$. The Landau expansion of the free energy in powers of the order parameter does not contain odd terms due to the time reversal symmetry. This suggests a second-order nature of the phase transition in MnSi, although fluctuations and interaction of the magnetic order parameter with other degrees of freedom could transform the phase transition into first-order [7–10][1)].

Another complication specific for the chiral spin systems is related to the spin and the chiral order coupling. If they were not coupled (see, e.g., [13, 14]), then one could expect two phase transitions in substances like MnSi, first to the spin ordered state, and then to the chiral state.

But despite theoretical conclusions and speculations, all physical properties of MnSi studied until very recently seemed to be continuous across the phase-transition line at ambient pressure (see [12] in this connection). Yet, the seemingly successful attempt of measuring some critical indexes at the phase transition in MnSi with a result hinting to the chiral universality class was made in Ref. [15].

The interest in studying MnSi was greatly enhanced by the finding that the temperature of the magnetic phase transition decreased with pressure and tended to zero at about 1.4 GPa with expectations of the quantum critical behavior [16]. Then, when a significant change was observed in the temperature dependence of *ac* susceptibility at the phase transition under high pressures, it was accepted as a manifestation of the existence of a tricritical point and first-order nature of the phase transition in MnSi at low temperatures and high pressures (12 K, 1.2 GPa) [17, 18]. This deduction was partly disputed on the basis of new measurements of the *ac* susceptibility and resistivity of MnSi at high pressures, created by compressed helium, and although the existence of a tricritical point at the phase transition line in MnSi was not denied, its location was shifted to the lower-pressure and higher-temperature domain (25.2 K, 0.355 GPa) [19, 20].

However, we note that an interpretation of the observations made at high pressure critically depends on the nature of the phase transition in MnSi at ambient pressure. Our extensive search in literature shows that there is no unambiguous evidence that allows classifying the transition as a second or a weak first-order one. Moreover, some remarkable properties of the phase transition in MnSi are not understood. In particular, some quantities like the thermal expansion coefficient [21], heat capacity [22], and temperature coefficient of resistivity [19] display a well-defined shoulders on the high-temperature side of their corresponding peaks at the phase transition, and the nature of these shoulders remains a puzzle. It is therefore appropriate to systematically investigate physical properties of MnSi with the same well-characterized sample. In the course of the study, the heat capacity, electrical resistivity, thermal expansion in magnetic fields, and *dc* and *ac* magnetic susceptibility of a high-quality MnSi single crystal were measured at ambient pressure.

2. EXPERIMENTAL

2.1. Sample preparation and its characteristics

The intermetallic compound MnSi is a congruently melting substance and its single crystals of good quality can be grown by direct crystallization from melt. The single crystal of MnSi used in the current study was grown by the Bridgman technique in a resistance furnace. Appropriate quantities of manganese (99.99% pure) and silicon (99.999% pure) were cleaned and arc-melted several times under an argon atmosphere. The alloy was then cast into a copper chill mold to ensure compositional homogeneity throughout the ingot, prior to crystal growth. The as-cast ingot was sealed in a quartz tube and heated under vacuum to 1100 °C. After reaching 1100 °C, the growth chamber was backfilled with ultra-high-purity argon to the pres-

[1)] The authors, having predicted a first-order transition in MnSi, claimed experimental support in Ref. [11]. Incidentally, the phase transition into the helical state in FeGe, which is structural and magnetic analogy of MnSi, is first order [12].

sure $1.03 \cdot 10^5$ Pa. Following pressurization, heating was continued until the ingot reached the temperature 1360 °C, and then held for one hour before being withdrawn from the furnace at a rate of 5 mm/hour. The ingot broke into several pieces after extraction from the quartz tube. The largest piece (20 mm in diameter and 40 mm height), examined by the X-ray Laue backreflection method, appeared to be a single crystal. Samples of the necessary size and orientation for various experiments were cut by low-power spark erosion.

Structural perfection of the MnSi single crystal was studied by means of a two crystal X-ray spectrometer. Rocking curve data were collected in the Θ-mode using the (110) MnSi reflection and Cu$K_{\alpha 1}$ radiation selected with a Si(400) monochromator. Overall mosaicity of the sample appeared to be less than 0.1°. The lattice constant of MnSi was measured with the Siemens D-500 X-ray diffractometer using CuK_α-radiation and the (440) reflection of the crystal in Θ–2Θ scanning mode. The measured doublet peak ($K_{\alpha_{1,2}}$) was fitted using the SPLIT PEARSON functions. For the lattice parameter of MnSi at 298 K ,we obtained $a = 4.5598(2)$ Å (to be compared with 4.5603(2) Å [23] and 4.559(1) Å [24]).

Elastic moduli of the given sample of MnSi, measured by the pulse ultrasound technique, are equal: $c_{11} = 283.30 \pm 1.62$ GPa, $c_{12} = 64.06 \pm 1.92$ GPa, and $c_{44} = 117.86 \pm 0.52$ GPa and the bulk modulus is $K = (c_{11} + 2c_{12})/3 = 137.14$ GPa [25]. The Debye temperature of MnSi, calculated from values of the elastic constants was found to be $\Theta_D \approx 500$ K. These values agree generally with earlier determinations [26].

To characterize purity of the samples, we measured the resistivity of a small splinter of the MnSi crystal with dimensions about $2 \times 0.7 \times 0.5$ mm^3 from room temperature to 50 mK[2]. The residual resistivity ratio (RRR) appeared to be equal to ≈ 250. From the saturated magnetization at high field at $T = 5$ K, the magnetic moment per atom Mn is $0.4\mu_B$; fitting low-field (0.1 T) inverse susceptibility data in the range 120–300 K to the Curie–Weiss form gives the effective moment $2.27\mu_B$ per Mn in the paramagnetic phase. These values agree well with previous reports (see the Inroduction). According to the results of the current experiments, the temperature of the phase transition in our sample of MnSi is confined to the limits 28.7–29 K.

[2] The splinter of MnSi was used to obtain a value of RRR to avoid complications related with possible contamination of the sample surface during cutting, polishing, and itching.

2.2. Experimental technique

dc magnetic susceptibility measurements were made in a Quantum design magnetic properties measurement system; *ac* susceptibility was measured with a two-coil set-up (drive and pick up coils) by a standard modulation technique at the modulation frequency 19 Hz. Heat capacity was measured with an adiabatic vacuum calorimeter by the heat pulse method. The overall accuracy of heat capacity measurements was about 1–1.5 %. Linear thermal expansion measurements were performed in a capacitance dilatometer with the resolution about 0.05 Å (see Ref. [27] for an extensive description of the technique). Resistivity measurements were carried out by a standard four-probe technique. In all these experiments, temperature was measured by calibrated Cernox thermometers with the overall resolution and accuracy not worse than 0.05 K. The heat capacity and thermal expansion measurements in magnetic fields were performed by using superconducting solenoids.

2.3. Experimental results

2.3.1. *Magnetic susceptibility.* *dc* and *ac* magnetic susceptibility data are plotted in Fig. 1*a*. The temperature derivative of the *dc* susceptibility is displayed in Fig. 1*b*. The unusual shape of $\chi(T)$ in the vicinity of the phase transition is seen in the inset of Fig. 1*a*. This form can be regarded as the result of a sudden jump-like increase in the magnetic susceptibility at the transition point, which is well demonstrated in Fig. 1*b*. Without this jump, the magnetic susceptibility curve would look like one typical of an antiferromagnetic phase transition.

2.3.2. *Heat capacity.* The heat capacity of MnSi divided by the temperature in the temperature range 2–40 K is shown in Figs. 2 and 3. We see that a sharp peak of C_p/T at ~ 28.8 K, looking as a slightly broadened delta function at the top of a rounded maximum, characterizes the phase transition in MnSi. We note that a sharp peak at the top of a rounded maximum (or a sharp dip at the bottom of a rounded minimum) is also seen in other properties of MnSi at the phase transition. Two more curves in Fig. 2 reflect the influence of the magnetic field on the heat capacity of MnSi. As is known, the magnetic field about 0.6 T at low temperature aligns spins in MnSi in the direction of the applied field, thus creating a field-induced ferromagnetic state [2]. Correspondingly, the magnetic field of a certain magnitude completely destroys the phase transition in MnSi, as is illustrated in Figs. 2 and 3. On

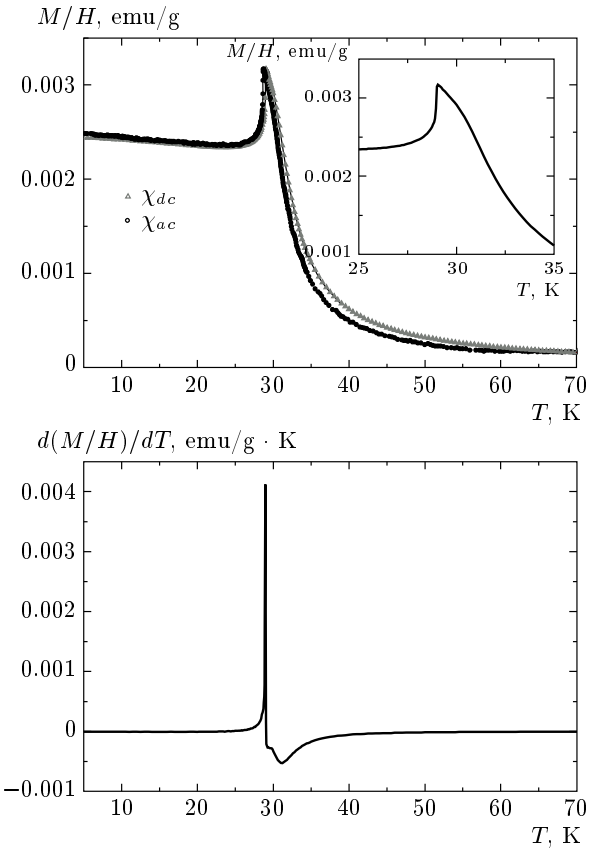

Fig. 1. The magnetic susceptibility $\chi = M/H$ of MnSi as a function of temperature. Measurements were made in a field of 1 mT at $H \parallel [110]$. The ac susceptibility data were scaled by simple multiplication

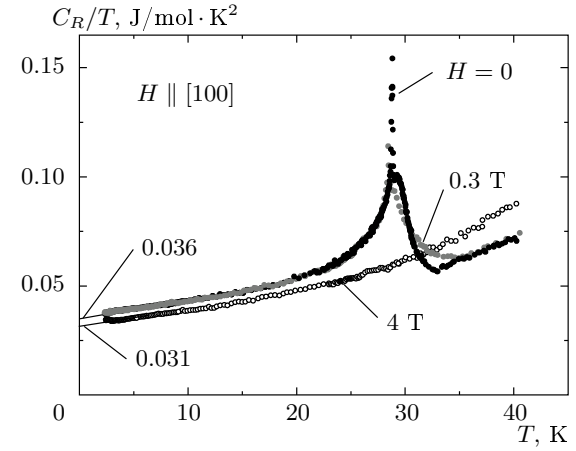

Fig. 2. Temperature dependence of the heat capacity divided by temperature in MnSi. Short extrapolations give values for the linear terms in the heat capacity $\gamma = 36$ mJ/mol·K^2 ($H = 0$) and $\gamma = 31$ mJ/mol·K^2 ($H = 4$ T)

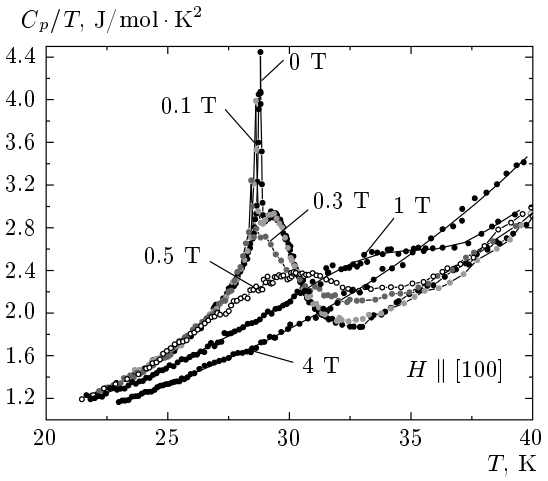

Fig. 3. Temperature dependence of the heat capacity divided by temperature near the phase transition in MnSi. It is seen that the heat capacity of the helical phase, is practically unaffected by magnetic fields up to 0.3 T

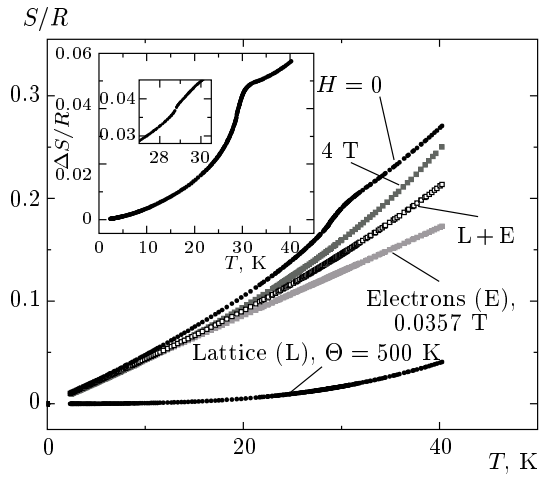

Fig. 4. The entropy of MnSi calculated from the heat capacity (R-gas constant). The electron contribution is taken in the conventional form as γT. The Debye model with $\Theta_D = 500$ K was used to estimate the lattice contribution to the entropy. The difference between the total entropy and the electron and phonon contributions $\Delta S = S - S_{el} - S_{ph}$ is shown in the inset. A tiny entropy jump at the phase transition is illustrated in the smaller inset

the other hand, moderate magnetic fields have little effect on the heat capacity of the helical phase even at the temperatures close to T_c. This last effect is not true for the paramagnetic phase, whose heat capacity readily responds to modest magnetic fields at temperatures close to and slightly above T_c.

We now turn to the low-temperature behavior of C_p/T. The standard way of analyzing heat capacity by plotting the data in the coordinates C_p/T vs. T^2 does not work in the present case because of the small phonon contribution (see Fig. 4). But the coefficient of the linear electronic term in the heat capacity of MnSi is easily obtained by extrapolating the low-temperature parts of the curves C_p/T to zero temperature in Fig. 2. The results yield $\gamma = 36$ mJ/mol·K^2 ($H = 0$) and 31 mJ/mol·K^2 ($H = 4$ T). The magnitude of γ for $H = 0$ is in good agreement with the earlier estimate, corrected for the obvious error in the order of the corresponding value [28]. Although the electron mass enhancement in MnSi is obvious from the high value of γ, the ratio m^*/m is unknown due to uncertainty in the electron concentration in MnSi. The calculated ideal value of γ_0 in the case with two free electrons for a molecule of MnSi is $\gamma_0 = 1.0$ mJ/mol·K^2, leading to the mass ratio $m^*/m \approx 36$ in MnSi.

The high values of the mass ratio in MnSi correlate with the electron mass enhancement in α-Mn[3)].

We next turn to Fig. 4, displaying behavior of the entropy S and its constituents in MnSi as a function of temperature. As is seen, the electronic contribution makes up a dominant fraction of the total entropy of MnSi due to high value of electron effective mass m^* (we neglect here a possibility of changing of m^* with temperature). At the same time, the calculated phonon contribution is rather small at the temperature range under study. The difference between the total entropy and the sum of electronic and phonon contributions, which characterizes the magnetic or spin ordering in MnSi, is less than 0.1 R (see the inset in Fig. 4), which once again identifies the itinerant nature of magnetism in MnSi.

2.3.3. *Thermal expansion.* Variation of the linear thermal expansion coefficient $\beta = (1/L_0)(dL/dT)$ of MnSi with temperature is shown in Fig. 5. Obviously, in the temperature range 0–35 K, behavior of β is defined by the magneto-volume and fluctuation effects arising as a result of the ordering of magnetic moments.

Plotting the data in coordinates β/T vs T^2 does not reveal any noticeable lattice contribution but exposes a remarkable linear temperature term in β in the temperature range 35–150 K (see the inset in Fig. 5), which probably correlates with the greatly enhanced electronic linear temperature term in the heat capacity.

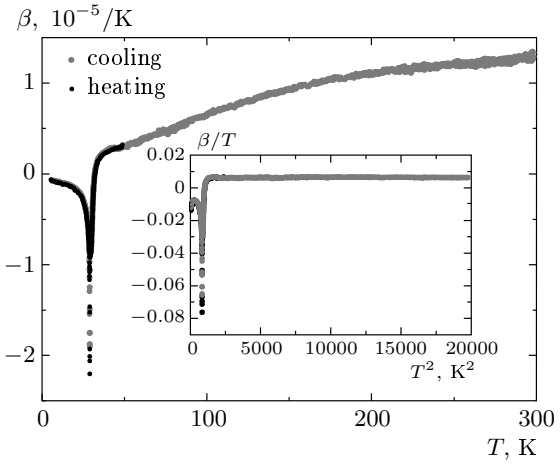

Fig. 5. Linear thermal expansion coefficient of MnSi (β). It is seen in the inset that the linear term dominates behavior of $\beta = (1/L_0)(dL/dT)$ in the range 30–100 K

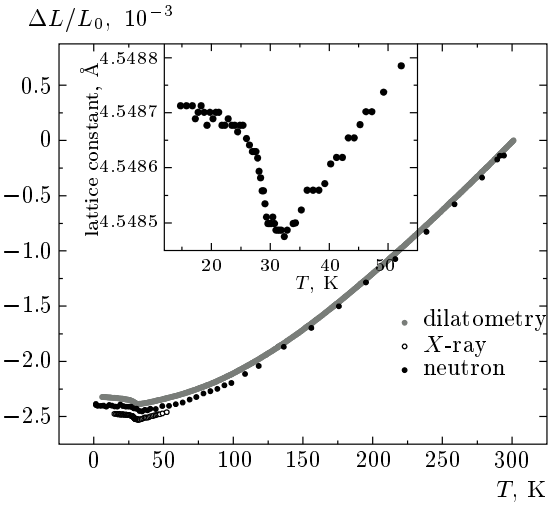

Fig. 6. Linear thermal expansion of MnSi

In Fig. 6, the thermal expansion $\Delta L/L_0(L_0 = L_{301\ \mathrm{K}})$ of MnSi, calculated by integration of the dilatometric data, is compared with powder neutron diffraction and single-crystal X-ray data [31]. As is seen, all the data agree within 0.02 %. The X-ray data set the absolute length scale, although they do not demonstrate enough resolution to permit observing subtle features of the phase transition as the dilatometric measurements do. Variation of the thermal expansion and the thermal expansion coefficient in the vicinity of the phase transition is shown in Fig. 7. The situation is fairly symmetric with respect to the heat capacity results. The sharp dip at the bottom of a shallow valley characterizes be-

[3)] With the number of free electrons per atom $Z = 2$, the lattice constant 8.912 Å, and the number of atoms in the unit cell $N = 58$ [29], we obtain $\gamma_0 = 0.6469$ mJ/mol·K^2. With the experimental value $\gamma = 12.812$ mJ/mol·K^2 [30] the mass ratio in α-Mn appears to be equal to $m^*/m \approx 20$.

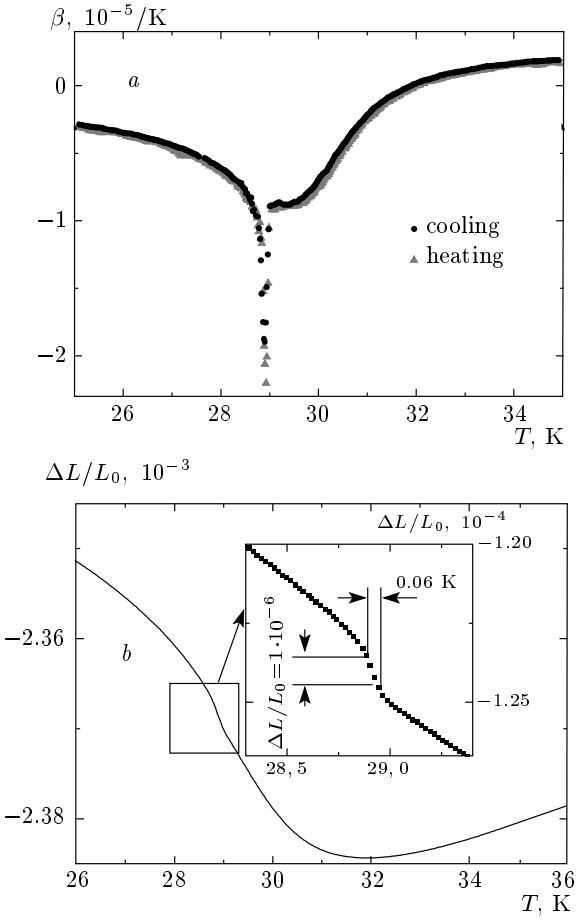

Fig. 7. Linear thermal expansion coefficient *a*) and linear thermal expansion of MnSi *b*) in the vicinity of the phase transition. Variation of the relative length of the sample close to the transition point is shown in the inset. For better view, a background contribution was subtracted from the original data. (The linear thermal expansion is calculated by integrating the thermal expansion coefficient)

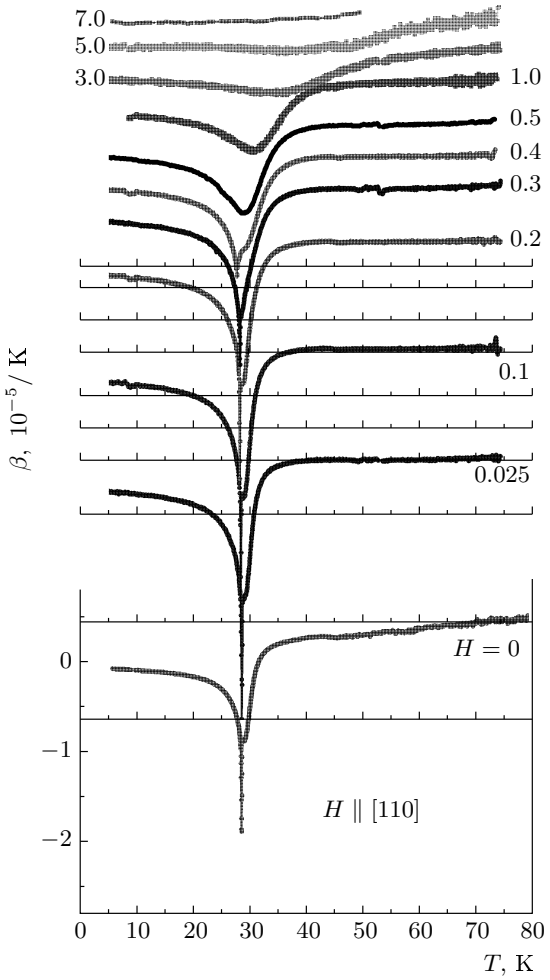

Fig. 8. Linear thermal expansion coefficient of MnSi in magnetic fields

havior of the thermal expansion coefficient around T_c in MnSi. Integration of the curve exposes a tiny anomaly that can be interpreted as a discontinuity of $1 \cdot 10^{-6}$ in $\Delta L/L_0$ at T_c and may indicate the first-order nature of the phase transition[4)]. This allows estimating the relative volume change at the first-order phase transition in MnSi as $3 \cdot 10^{-6}$. Using the Clausius–Clapeyron equation and taking the slope of the transition line from Ref. [19], we obtain the corresponding entropy change $5 \cdot 10^{-4}\ R$ (R is the gas constant). This value agrees with the direct estimate that can be made from the entropy variation through the phase transition (Fig. 4).

Now we turn to Fig. 8, which illustrates the influence of the magnetic field on the thermal expansion coefficient of MnSi. In the case of the helical spin ordering, the magnetic field is not directly coupled to the order parameter, and hence no significant effect of the magnetic field on the phase transition is expected until the field-induced ferromagnetic state appears at about 0.35 T [32]. As can be seen in Fig. 8, moderate magnetic fields up to 0.025 T even sharpen the phase transition (probably as a result of forming a single domain sample, see Fig. 9). Then the fast degradation of sharp features of the transition between 0.3–0.4 T clearly indicates formation of the ferromagnetic spin

[4)] Simple consideration leads to the following approximate formula for the thermodynamic temperature hysteresis: $\delta T = K(\Delta V/V)/(dT/dP)$, where K is the bulk modulus, $\Delta V/V$ is the relative volume change, and dT/dP is the slope of the transition line. Using the numerical values $K = 1.37 \cdot 10^6$ bar [23], $\Delta V/V = 3 \cdot 10^{-6}$, $dT/dP = 1.1 \cdot 10^{-3}$ K/bar [19] we obtain 0.005 K for the hysteresis, which is a rather low value that hardly can be observed in the current conditions.

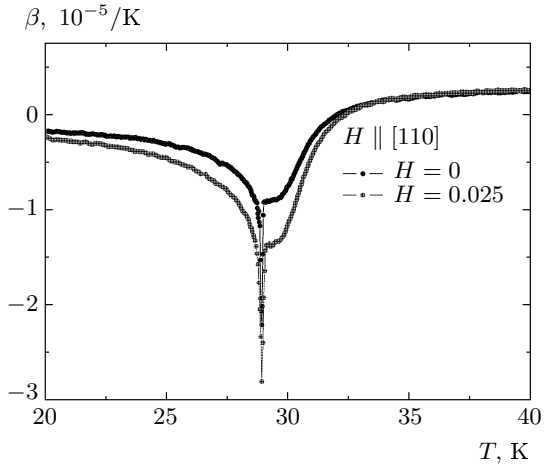

Fig. 9. Influence of a weak magnetic field (2.5 mT) on the thermal expansion coefficients of MnSi

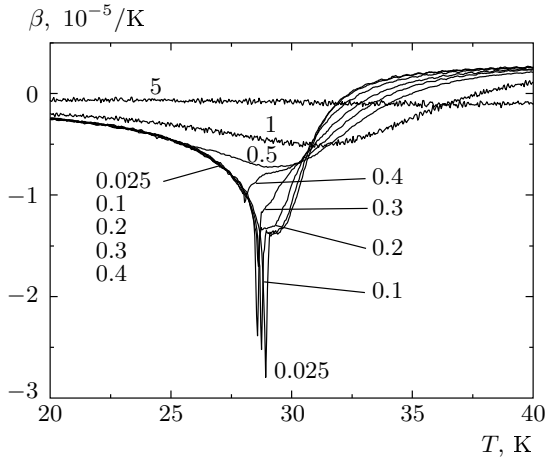

Fig. 10. The linear thermal expansion coefficient of MnSi near the phase transition in magnetic fields. It is seen that moderate magnetic fields up to 0.4 T do not influence thermal expansion of the helical phase

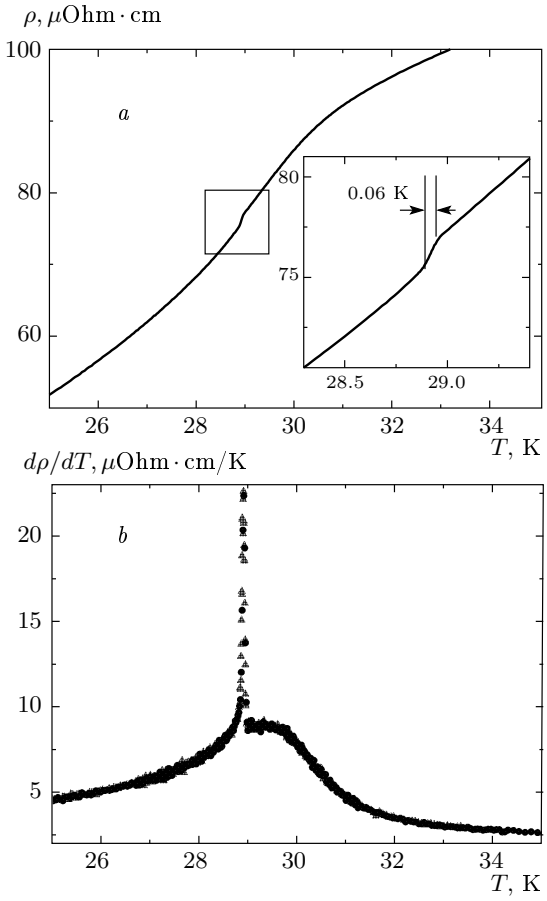

Fig. 11. Variations of resistivity (a) and its temperature derivative (b) of MnSi with temperature. The quasi-discontinuity at the phase transition point is shown in the inset. Improved results compared to those in Ref. [20] were obtained due to the higher quality sample, the optimized sample dimensions and the better temperature control

structure. Figure 10 indicates that although magnetic fields less than 0.4 T do not change nature of the phase transition, they strongly influence thermal expansion of the paramagnetic phase. At the same time, thermal expansion of the helical phase shows little to no change at least up to 0.4 T. The same situation can also be seen in the heat capacity of the MnSi response to moderate magnetic fields (Fig. 2, 3). This implies a significant stiffness of the helical spin structure or, in the other words, a lack of extensive paramagnetic fluctuations in MnSi even at the transition point. This most probably signifies a finite value of the order parameter at the phase transition point, therefore confirming a discontinuous nature of the phase transition in MnSi.

2.3.4. *Electrical resistivity, heat capacity, and thermal expansion relations.* At a first glance, the overall dependence of the resistivity of our sample of MnSi on temperature $\rho(T)$ in the vicinity of the phase transition does not differ from numerous previous results (see, e.g., [16–18]); however, a small quasi-discontinuity can clearly be seen at $T = 28.9$ K (Fig. 11). The corresponding temperature derivatives of the resistivity can be interpreted as a slightly broadened delta function developing within the continuous anomaly, similarly to the behavior of the heat capacity and the thermal expansion coefficient. Almost perfect similarity between the temperature derivative of the resistivity, the heat

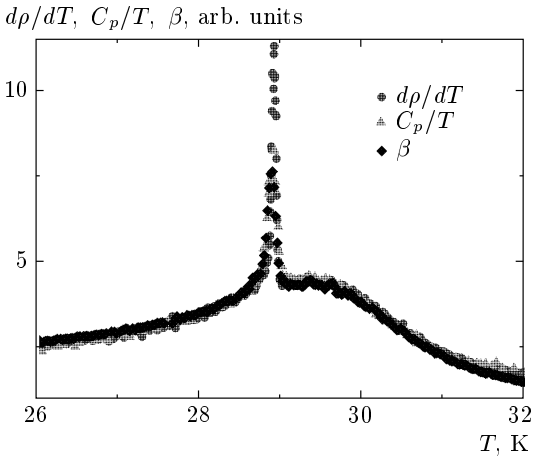

Fig. 12. Unified dependence of the heat capacity, the temperature derivative of resistivity and the linear thermal expansion coefficient of MnSi in the phase-transition region on temperature. All curves were reduced by a linear transformation. The data for the thermal expansion coefficient were taken with the inverse sign

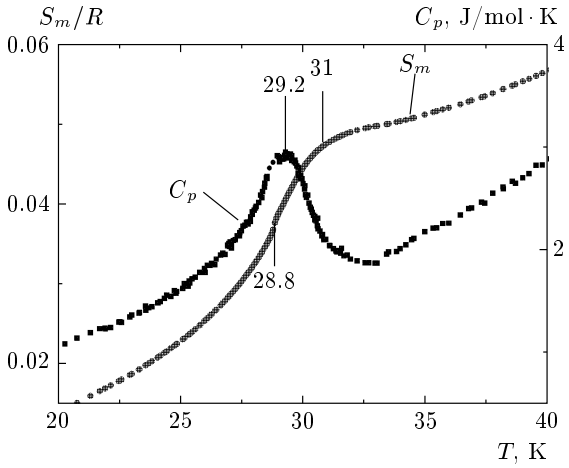

Fig. 13. The magnetic part of entropy S_m/R and heat capacity C_p of MnSi in the vicinity of the phase transition. The peak in C_p was eliminated for the better view of the rounded maximum

capacity, and the linear thermal expansion coefficient curves in the phase transition region (see [33–35] in this connection) is displayed in Fig. 12.

3. CONCLUSION

As can be seen from Figs. 2, 3, 7, and 11, a sharp peak on the low-temperature side of the rounded maximum or correspondingly a sharp dip to the left of the bottom of the rounded minimum in the heat capacity, the thermal expansion coefficient, and temperature derivatives of resistivity is an intrinsic property of the phase transition in the itinerant helical magnet of MnSi. Striking similarity between all these quantities is evident from the reduced curve in Fig. 12. This obviously indicates spin fluctuations as a dominant factor defining thermodynamic and transport properties of MnSi in the vicinity of the phase transition.

The sharp peaks observed in the mentioned quantities most likely identify the phase transition in MnSi as a weakly first-order transition. This conclusion is certainly supported by our claim of a finite value of the order parameter at the transition temperature (see Sec. 3.3). It is also appropriate to refer to the well-forgotten result in Ref. [11], where a finite value of the critical magnetic field corresponding to the transition from the conical to the ferromagnetic spin structure at the phase transition temperature was found. It must be mentioned here that as was explicitly shown in Ref. [36], the second-order phase transition in the itinerant weak ferromagnet $ZrZn_2$ displayed typical mean-field behavior with simple jumps in C_p and $d\rho/dT$ at the phase transition point. This clearly supports up our interpretation of the nature of the phase transition in MnSi.

Then a number of questions arises. If one believes that a tricritical point does exist at high pressure in MnSi [17–19], then the only way is to suggest that the phase transition becomes second order at high pressure. This kind of conclusions would completely reverse the widely accepted view of the phase diagram of MnSi.

Alternative scenarios, which principally could be discussed, include the existence of a second tricritical point[5)] or interplay of weak and strong first-order transitions [37], but it is unclear whether the latter would generate some sort of pseudo-tricritical point. Another intriguing possibility in the chiral spin systems is decoupling the spin and the chiral orders, which may lead to two phase transitions, first to the spin ordered state and then to the chiral state (see, e.g., [13, 14]). But the above consideration ignores the question on the nature of the rounded maxima demonstrated in Fig. 12. Some insight comes from the behavior of the magnetic part of the entropy and the heat capacity, with the peak eliminated, through the phase transition in MnSi (Fig. 13).

As can be seen from the entropy curve, some order-

[5)] In principle, two tricritical points may exist on the transition line for materials like MnSi; however, a competing spin order should be observed in this case [8].

ing process starts around 31 K, reaches its culmination at the temperature corresponding to the top of the rounded maximum of C_p (29.2 K), and is interrupted by the first-order phase transition a half of degree below (28.8 K). The overall behavior of the entropy and the heat capacity looks like the system is preparing to take some sort of frustrated magnetic configuration but then some subtle interaction comes into play and the system collapses into the helical phase. We are not in a position to discuss a character of this interaction here, but perhaps fourth energy scale is needed to unlock the configuration space, therefore facilitating the phase transition in MnSi[6)]. Going a little bit beyond the scope of the current paper, we may expect that a cloud of the "frustrated phase" follows the phase transition line until the very end at $T = 0$ at high pressure and then it may condense into the extended quantum phase with non-Fermi-liquid properties.

The authors are grateful to I. E. Dzyaloshinski, S. V. Maleev, and S. A. Brazovsky for the discussion and valuable remarks. Technical assistance of J. D. Thompson, V. Sidorov, and V. V. Krasnorussky is greatly appreciated. DW and TAL wish to acknowledge the support of the U. S. Department of Energy, Basic Energy Sciences. S. M. S. and A. E. P. appreciate support of the RFBR (grant 06-02-16590), Program of the Physics Department of RAS on Strongly Correlated Systems and Program of the Presidium of RAS on Physics of Strongly Compressed Matter. Work at Los Alamos was performed under the auspices of the US Department of Energy, Office of Science.

REFERENCES

1. H. J. Williams, J. H. Wernick, R. C. Sherwood, and G. K. Wertheim, J. Appl. Phys. **37**, 1256 (1966).
2. J. H. Wernick, G. K. Wertheim, and R. C. Sherwood, Mat. Res. Bull. **7**, 1431 (1972).
3. B. Borén, Ark. Kemi Min. Geol. **11A**, 1 (1933).
4. I. Dzyaloshinski, J. Phys. Chem. Sol. **4**, 241 (1958).
5. T. Moriya, Phys. Rev. **120**, 91 (1960).
6. Y. Ishikawa, K. Tajima, D. Bloch, and M. Roth, Sol. St. Comm. **19**, 525 (1976).
7. S. A. Brazovskii, I. E. Dzyaloshinski, and B. G. Kukharenko, Zh. Eksp. Theor. Phys. **70**, 2257 (1976) [Sov. Phys. JETP **43**, 1178 (1976)].
8. I. E. Dzyaloshinski, Zh. Eksp. Theor. Phys. **72**, 1930 (1977) [Sov. Phys. JETP **45**, 1014 (1977)].
9. Per Bak and M. Høgh Jensen, J. Phys C: Sol. St. Phys. **13**, L 881 (1980).
10. A. I. Larkin and S. A. Pikin, Sov. Physics, JETP-USSR **29**, 891 (1969).
11. Y. Ishikawa, T. Komatsubara, and D. Bloch, Physica **86–88B**, 401 (1977).
12. P. Pedrazzini, H. Wilheim, D. Jaccard et al., Phys. Rev. Lett. **98**, 047204 (2007).
13. H. T. Diep, Phys. Rev. B **39**, 397 (1989).
14. M. L. Plumer and A. Mailhot, Phys.Rev. B **50**, 16113 (1994).
15. S. V. Grigoriev, S. V. Maleyev, A. I. Okorokov, Yu. O. Chetverikov, R. Georgii, P. Böni, D. Lamago, H. Eckerlebe, and K. Pranzas, Phys. Rev. B **72**, 134420 (2005).
16. J. D. Thompson, Z. Fisk, and G. G. Lonzarich, Physica B **161**, 317 (1989).
17. C. Pfleiderer, G. J. McMullan, and G. G. Lonzarich, Physica B **206–207**, 847 (1995).
18. C. Pfleiderer, G. J. McMullan, S. R. Julian, and G. G. Lonzarich, Phys. Rev. B **55**, 8330 (1997).
19. A. E. Petrova, V. Krasnorussky, J. Sarrao, and S. M. Stishov, Phys. Rev. B **73**, 052409 (2006).
20. A. E. Petrova, E. D. Bauer, V. Krasnorussky, and S. M. Stishov, Phys. Rev. B **74**, 092401 (2006).
21. M. Matsunaga, Y. Ishikawa, and T. Nakajima, J. Phys. Soc. Jpn. **51**, 1153 (1982).
22. D. Lamago, R. Georgii, C. Pfleiderer, and P. Böni, Physica B **385–386**, 385 (2006).
23. J. E. Jorgensen and S. Rasmussen, Powder Diffraction **6**, 194 (1991).
24. S. Okada, T. Shishido, Y. Ishizawa, M. Ogawa, K. Kudou, T. Fukuda, and T. Lundström, J. Alloys and Compounds **317–318**, 315 (2001).
25. E. L. Gromnitskaya, private communication.
26. G. P. Zinoveva, L. P. Andreeva, and P. V. Geld, Phys. Stat. Sol. **23**, 711 (1974).
27. G. M. Schmiedeshoff, A. W. Lounsbury, D. J. Luna, S. J. Tracy, and A. J. Schramm, S. W. Tozer, V. F. Correa, S. T. Hannahs, T. P. Murphy, E. C. Palm, A. H. Lacerda, S. L. Bud'ko, P. C. Canfield, J. L. Smith, J. C. Lashley, and J. C. Cooley, Rev. Sci. Instrum. **77**, 123907 (2006).

[6)] Striction effects might also be relevant to this case [10].

28. E. Fawcett, J. P. Maita, and J. H. Wernick, Intern. J. Magnetism **1**, 29, (1970).

29. Natl. Bur. Stand.(US) Monogr. **25**, 17, 50 (1980).

30. G. L. Guthrie, S. A. Friedeberg, and J. E. Goldman, Phys. Rev. **139**, A1200 (1965).

31. B. Fåk, J. Flouquet, and G. Lapertot, J. Phys.: Condens. Matter **17**, 1635 (2005). R. A. Sadykov, private communication.

32. S. V. Grigoriev, S. V. Maleyev, A. I. Okorokov, Yu. O. Chetverikov, and H. Eckerlebe, Phys. Rev. B **73**, 224440 (2006).

33. V. M. Nabutovskii and A. Z. Patashinskii, Fizika Tverdogo Tela **10**, 3121 (1968).

34. M. E. Fisher and J. S. Langer, Phys. Rev. Lett. **20**, 665 (1968).

35. T. G. Richard and D. J. W. Geldart, Phys. Rev. Lett. **30**, 290 (1973).

36. E. A. Yelland, S. J. C. Yates, O. Taylor, A. Griffiths, S. M. Hayden, and A. Carrington, Phys. Rev. B **73**, 184436 (2005).

37. T. Vojta and R. Sknepnek, Phys. Rev. B **64**, 052404 (2001).